

MULTIDISCIPLINARY DESIGN EXPLORATION OF HYBRID-ELECTRIC REGIONAL AIRCRAFT

Salvatore Trepiccione[1], Giuseppe Melone[1], Fabrizio Nicolosi[1], Giuseppe Piscopo[2] & Mario Di Stasio[1]

[1]University of Naples Federico II, Department of Industrial Engineering, Via Claudio 21, Naples, 80125, Italy
[2]Leonardo S.p.A., Preliminary Design Office, Viale dell'Aeronautica s.n.c., Pomigliano d'Arco, 80038, Italy

Abstract

This work compares hydrogen fuel-cell with conventional kerosene turboprop propulsion for regional aircraft in a 2040 entry-into-service timeframe. Using a multidisciplinary design optimization workflow within the Hybrid Electric Aircraft Research Tool (HEART) framework, six configurations spanning 80 and 100 passengers are analyzed over a 500 nm design range: conventional kerosene turboprop (K80, K100), hydrogen fuel-cell electric (H80, H100), and hybrid-electric variants combining kerosene and cryogenic hydrogen propulsion (KH80, KH100). The study demonstrates how the payload class and the choice of propulsion system jointly determine the design feasibility and competitiveness of hydrogen-based and hybrid solutions.

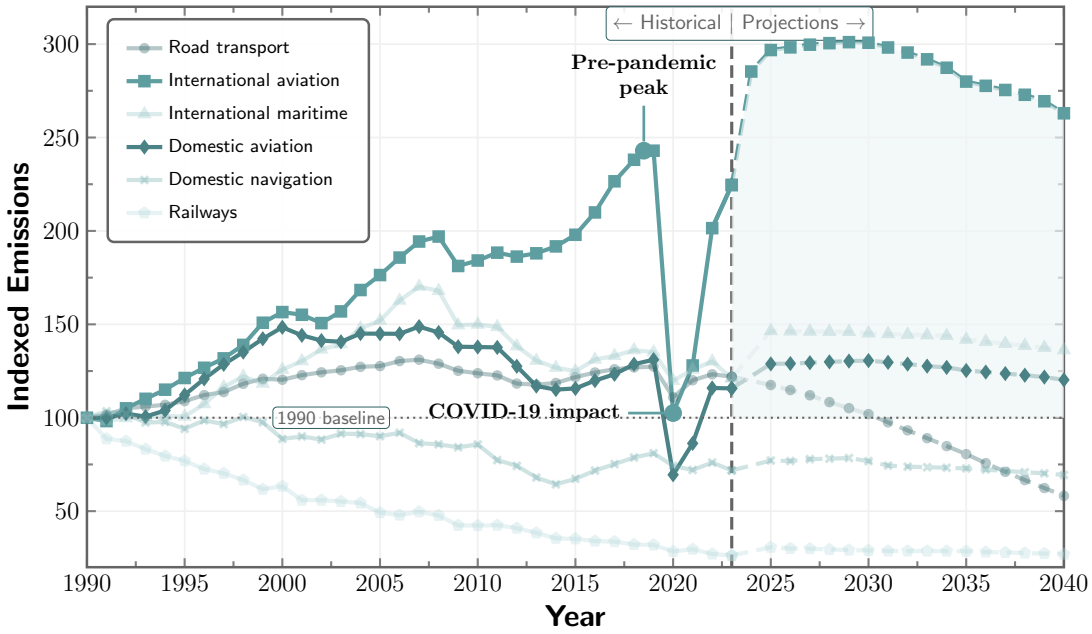
Keywords: hydrogen fuel cell, hybrid-electric, regional aircraft, multidisciplinary design optimization, cryogenic storage

1. Introduction

Aviation accounts for approximately 2.5 % of global anthropogenic CO_2 emissions and a disproportionately larger share of effective radiative forcing when non-CO_2 effects are included [1]. The EU Green Deal, CORSIA, and Fit-for-55 collectively call for a 55 % net reduction in aviation emissions by 2030 relative to 1990 levels, with a net-zero ambition by 2050. As illustrated in Figure 1, transport-sector greenhouse-gas emissions have not declined uniformly across modes, with aviation remaining a significant contributor; incremental improvements to conventional kerosene turboprop architectures are insufficient to meet these targets.

The regional aircraft segment is a particularly attractive target for zero-emission propulsion [2]: its short stage lengths and moderate payload levels are more compatible with the integration constraints of emerging technologies than long-haul operations. Liquid hydrogen (LH_2) has emerged as a leading candidate [3, 4]: its gravimetric energy density exceeds jet fuel by a factor of three; combustion produces water vapour rather than CO_2; and electrolysis-derived green hydrogen approaches zero life-cycle carbon intensity. Polymer-electrolyte-membrane (PEM) fuel cells convert H_2 to shaft power at efficiencies surpassing gas-turbine cycles at regional aircraft power ratings. The present study adopts a 2040 entry-into-service horizon, consistent with technology readiness projections for MW-class fuel-cell propulsion systems.

Prior work provides both methodological context and domain-specific precedent. Automated geometry generation and aircraft performance-analysis tools are documented in De Marco et al. [5, 6], and a preliminary sizing assessment of hydrogen-powered regional concepts is reported in Di Stasio et al. [7]. Model-based systems engineering and collaborative multidisciplinary design optimization have been demonstrated on blended-wing-body configurations [8] and business-jet families [9] within the AGILE EU project, providing methodological context for the integrated workflow adopted here. Building on this foundation, Rischmüller et al. [10] reported a 13 % fuel-consumption reduction



Source: European Environment Agency (EEA) — National emissions reported to UNFCCC and EU Governance Regulation

Figure 1 – Indexed greenhouse-gas emissions by European transport mode, 1990–2040.

for a dual-fuel hybrid D328eco at the cost of significant payload penalty, while Palladino et al. [11] demonstrated fuel-burn reductions above 30 % per passenger for a 70-seat hydrogen hybrid turboprop, identifying thermal management as the key design driver; a multidisciplinary optimization of a more-electric regional aircraft incorporating explicit certification constraints is reported by Fioriti et al. [12].

This paper presents a comparative sizing study of six regional aircraft configurations, covering 80- and 100-passenger variants across three propulsion architectures: conventional kerosene turboprop, hydrogen fuel-cell electric, and an hybrid-electric combining kerosene and cryogenic hydrogen — all designed for a 500 nm design range. A unified automated framework drives the exploration and optimization of each configuration within a single environment, enabling a consistent assessment of how payload class and propulsion type jointly shape the optimum design, with particular attention to the contrasting role of wing aspect ratio across the three families of design spaces.

The paper is organized as follows. Section 2. describes the multidisciplinary workflow in detail.Section 3. defines the six aircraft configurations and the DOE parameter space employed in the study. Section 4. presents and discusses the response-surface results, the constraint analysis, and the identified optimal configurations. Concluding remarks follow in Section 5..

2. Methodology

This study adopts a multidisciplinary aircraft design workflow implemented within the HEART framework to generate a response surface for a conventional or hydrogen-powered regional aircraft configuration. The framework integrates aircraft geometry synthesis, weight estimation, centre-of-gravity analysis, aerodynamic assessment, mission performance simulation, and constrained optimization within a unified iterative process, as illustrated in Figure 2. The computational framework is organized into two nested iterative levels. The outer loop performs a Design of Experiments (DOE) sweep across the principal aircraft design variables, while the inner loop performs mission-fuel convergence and — for hydrogen-powered configurations — hydrogen storage geometry reconciliation.

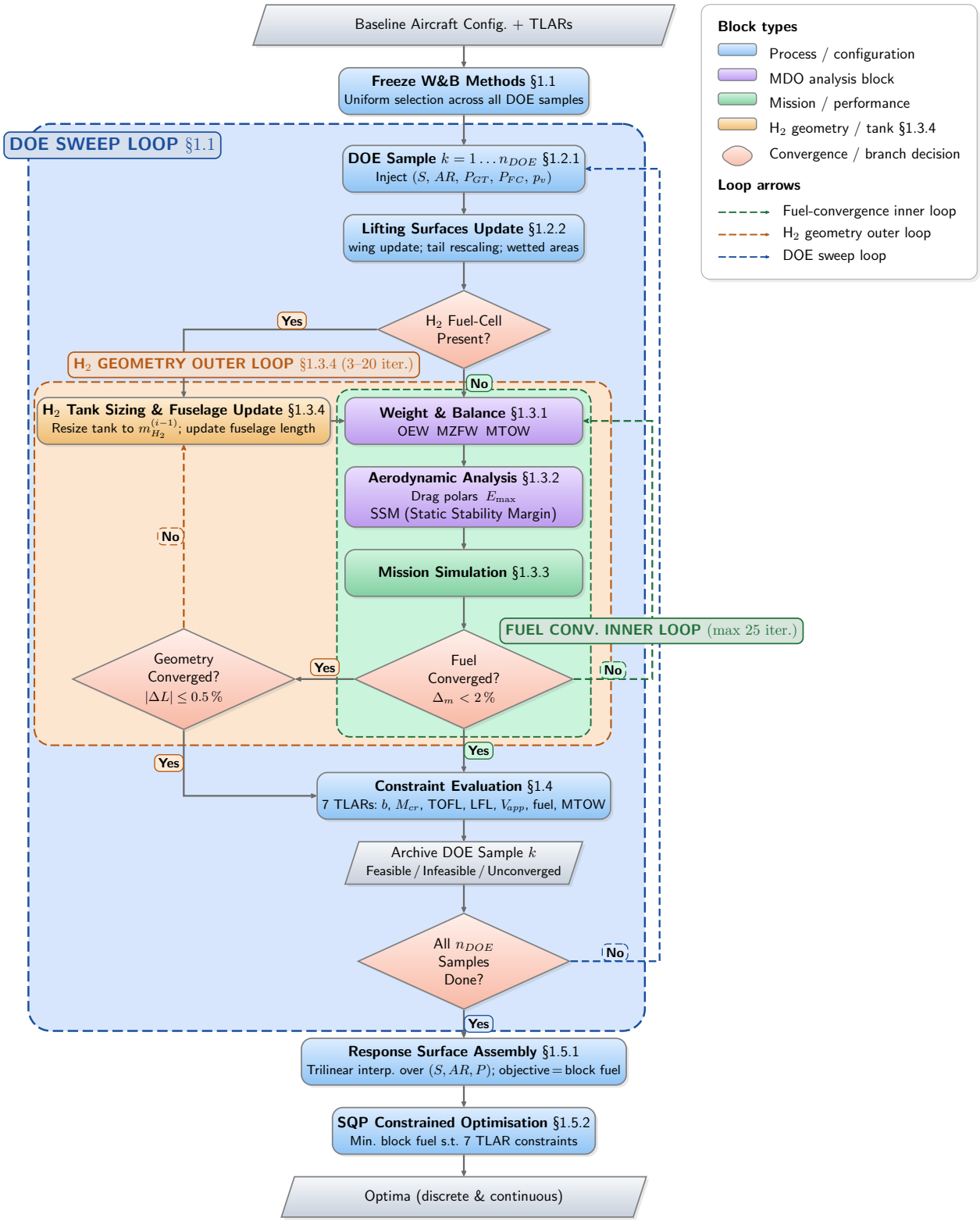


Figure 2 – MDO workflow: DOE sweep loop, fuel-convergence inner loop, and H_2 geometry outer loop.

2.1 Technological Assumptions

The present study adopts a 2040 entry-into-service technology horizon, consistent with the maturation roadmap for MW-class fuel-cell propulsion systems [13]. Table 1 summarises the key technological assumptions imposed on the propulsion and powertrain components across all the configurations. These assumptions directly enter the HEART component-weight models and drive the feasible design spaces described in Sections 3. and 4.. Fixed aerodynamic and empennage configuration parameters shared across all six configurations are collected in Table 2. Cryogenic tank design specifications, which are specific to hydrogen configurations, are reported separately in Table 3.

Table 1 – Key technological assumptions for the propulsion and powertrain components at the 2040 EIS horizon. Cryogenic tank assumptions are reported separately in Table 3.

Component	Parameter	Assumed Value
Gas Turbine		
	Power density	$10\ \mathrm{kW\,kg^{-1}}$
PEM Fuel-Cell System		
	System-level specific power	$2.0\ \mathrm{kW\,kg^{-1}}$
	System efficiency (at rated power)	$55\,\%$
Electric Motor		
	Power density	$15\ \mathrm{kW\,kg^{-1}}$
	Efficiency	$98\,\%$
	High voltage bus interface	$800\ \mathrm{V_{DC}}$
HV Inverter		
	Power density	$15\ \mathrm{kW\,kg^{-1}}$
	Efficiency	$98\,\%$
Propeller		
	Power density	$12.5\ \mathrm{kW\,kg^{-1}}$
Propeller Gearbox		
	Mechanical efficiency	$97\,\%$
	Power density	$11.1\ \mathrm{kW\,kg^{-1}}$

Table 2 – Fixed aerodynamic and empennage configuration parameters shared across all six aircraft configurations. Values are held constant throughout the DOE sweep.

Component	Parameter	Assumed Value
Lift coefficients — all configurations		
	$C_{L,\max}$ at take-off	2.35
	$C_{L,\max}$ at landing	2.65
Empennage — all configurations		
	Horiz. tail vol. coeff. V_H	1.360
	Vert. tail vol. coeff. V_V	0.093

The multidisciplinary workflow described above is applied to six distinct aircraft configurations, whose naming convention reflects both propulsion architecture and seating capacity. **K80** and **K100** denote the 80- and 100-passenger conventional kerosene turboprop variants, each powered by twin gas-turbine engines; **H80** and **H100** denote the corresponding hydrogen fuel-cell-electric variants, featuring cryogenic rear-fuselage tanks and four propulsion units each; and **KH80** and **KH100** denote the hybrid-electric variants, combining kerosene gas-turbine and hydrogen fuel-cell propulsion together with cryogenic rear-fuselage hydrogen storage, powered by two propulsion units with a turboelectric architecture. All six configurations share a 500 nm design mission range; complete descriptions and top-level requirements are presented in Section 3..

2.2 Design Variables and Design Space Definition

The response surface is constructed via a structured DOE whose dimension depends on the propulsion architecture. For **conventional kerosene** configurations, the three-dimensional design vector is $\mathbf{x}_{\mathrm{K}} = \left(S,\, AR,\, P_{\mathrm{GT}}\right)^{\top} \in \mathscr{X}_{\mathrm{K}} \subset \mathbb{R}^3$; for **hydrogen fuel-cell** configurations the four-dimensional design vector is $\mathbf{x}_{\mathrm{H}} = \left(S,\, AR,\, P_{\mathrm{FC}},\, p_v\right)^{\top} \in \mathscr{X}_{\mathrm{H}} \subset \mathbb{R}^4$; and for **hybrid-electric** configurations the five-dimensional design vector is $\mathbf{x}_{\mathrm{KH}} = \left(S,\, AR,\, P_{\mathrm{GT}},\, P_{\mathrm{FC}},\, p_v\right)^{\top} \in \mathscr{X}_{\mathrm{KH}} \subset \mathbb{R}^5$. The components are:

(i) wing planform area S [m^2] — shared across all architectures;

(ii) wing aspect ratio AR — shared across all architectures;

(iii) gas-turbine engine power P_{GT} [W] — kerosene and hybrid configurations;

(iv) fuel-cell system power P_{FC} [W] — hydrogen and hybrid configurations;

(v) hydrogen tank venting pressure p_v [bar] — hydrogen and hybrid configurations.

The DOE is a fully enumerated Cartesian product over the active variables of each architecture:

$$n_{\mathrm{DOE}} = \begin{cases} \displaystyle\prod_{i \in \{S, AR, P_{\mathrm{GT}}\}} n_i & \text{(kerosene)} \\ \displaystyle\prod_{i \in \{S, AR, P_{\mathrm{FC}}, p_v\}} n_i & \text{(hydrogen)} \\ \displaystyle\prod_{i \in \{S, AR, P_{\mathrm{GT}}, P_{\mathrm{FC}}, p_v\}} n_i & \text{(hybrid)} \end{cases} \tag{1}$$

Evaluating Eq. (1) yields 252 design evaluations per kerosene configuration (504 combined for K80 and K100), 600 evaluations per hydrogen configuration (1200 combined for H80 and H100) and 39 evaluations per hybrid-electric configuration (78 combined for KH80 and KH100). The current campaign covers 1743 HEART simulations for the six pure-architecture configurations (K80, K100, H80, H100, KH80, KH100); the total will be revised once the hybrid DOE grid is finalised. For each DOE

sample, wing geometry is updated from the prescribed planform area and fixed aspect ratio; horizontal and vertical tail areas are rescaled to preserve the baseline volumetric stability coefficients V_H and V_V.

2.3 Multidisciplinary Convergence Workflow

For each DOE point, an iterative convergence process branches on the propulsion configuration: **Branch A** (hydrogen) employs an outer geometry-convergence loop (tank sizing and fuselage-length adaptation) wrapping an inner fuel-weight loop; both must converge simultaneously. **Branch B** (kerosene) uses only the inner fuel-weight loop, since kerosene storage does not drive fuselage geometry adaptation. **Branch C** (hybrid) combines both: the outer geometry-convergence loop handles cryogenic hydrogen tank sizing and fuselage adaptation, while the inner fuel-weight loop converges both the kerosene and hydrogen block masses simultaneously; for the solution to be accepted, both fuel-mass residuals (Eq. (2)) must be satisfied concurrently. At each inner-loop iteration, aircraft masses (OEW, MZFW, MTOW) are recomputed, the centre-of-gravity envelope is updated, and trimmed lift curves, drag polars, and static stability margins are recomputed at multiple CG conditions.

2.3.1 Mission Performance Simulation and Fuel Convergence

Mission performance is evaluated by a segment-based framework coupled to the propulsion system model. The mission profile comprises taxi-out, climb, cruise, descent, landing, taxi-in, and reserve fuel evaluation, consistent with the 500 nm design range. During each inner-loop iteration, the mission analysis computes the kerosene and hydrogen mass consumed for the current aircraft state, with energy conservation verified at the end of each evaluation.

Fuel convergence is assessed independently for each active fuel type. The relative fuel-mass residual at iteration i is defined as:

$$\Delta_{m,\tau}^{(i)} = \frac{\left| m_\tau^{(i)} - m_\tau^{(i-1)} \right|}{m_\tau^{(i-1)}} \times 100 \; < \; \varepsilon \tag{2}$$

where the subscript $\tau \in \{\text{kerosene}, \text{hydrogen}\}$ identifies the fuel type and $\varepsilon = 2.0\%$ is the prescribed convergence threshold. The inner loop terminates only when the residuals for *both* active fuel types simultaneously satisfy this criterion. If a propulsion subsystem is absent from the configuration, the corresponding residual is set to zero and excluded from the convergence check. A safety cap of 25 inner-loop iterations is enforced to prevent non-termination in degenerate cases.

After each mission evaluation, the predicted fuel masses are re-injected into the aircraft inertia model and MTOW is updated as:

$$\text{MTOW}^{(i)} = \text{MZFW} + m_{\text{fuel,total}}^{(i)} \tag{3}$$

For hybrid-electric configurations, $m_{\text{fuel,total}}^{(i)} = m_{\text{ker}}^{(i)} + m_{\text{H}_2}^{(i)}$ is the sum of the block kerosene and block hydrogen masses; both residuals are tracked independently via Eq. (2) and must simultaneously satisfy the convergence criterion before the MTOW update is accepted. The multidisciplinary loop is then repeated until convergence is achieved.

2.3.2 Hydrogen Tank Sizing and Geometry Adaptation

The preliminary design of the cryogenic tank is carried out through an object-oriented workflow developed in the MATLAB environment. The architecture of the framework evaluates the geometric, thermo-fluid dynamic, and structural aspects of the tank in a coupled manner, in order to estimate the overall tank geometry and mass, together with the total stored hydrogen mass. The total hydrogen mass accounts for the block mission, reserve and contingency (both expressed in percentage of the block mission contribution), and vented hydrogen masses, whereas the overall tank system mass is the sum of the structural components (including heaters) and ancillaries (pumping system, sensors, valves, filling and venting lines) masses. The mass of the latter is estimated as a percentage of the total structural mass.

The tank section and enclosure shapes must be selected a priori, as well as the insulation system and the operative conditions of the tank, such as fuel flow and altitude time histories. In the present study, a double-wall jacketed MLI insulated configuration was selected for the tank. For such layouts, a vacuum condition is reached between the two liners; therefore, the structural sizing of the two liners is performed in two different ways: the inner liner is sized for an expansion load adopting the analytical model for hoop stress [14], whereas the outer liner is sized for compression and buckling loads, according to the AD 2000 guidelines [15].
The thermal module, based on a one-dimensional electrical analogy model that treats hydrogen as a homogeneous mixture [16, 17], calculates the pressure levels reached during flight. This enables the estimation of the total vented hydrogen mass, required to allow safe tank operations, and the overall mass of heaters for a given set of operative pressure ranges. The structural and thermal modules are used in a coupled manner, in order to find the minimum insulation thickness able to satisfy the dormancy and structural integrity requirements.

Table 3 – Cryogenic tank design specifications and surrogate model development parameters. The maximum pressure level corresponds to the venting pressure, which is used as design variable in the current DOE study. Differently, the tank inner diameter refers to the diameter of the inner tank structure effectively storing the hydrogen mass.

Assumption / Parameter	**Primary Tank**	**Secondary Tank**
Tank geometry	Cylindrical	Conical
Tank cross-section	Circular	
Tank enclosure	Elliptical	
Inner and outer liner material	Aluminium 2219	
Limit stress (MPa)	172.6	
Structural Safety factor	3.00	
Minimum pressure level (bar)	1.2	

Design Variable	**Symbol**	**Variation Range**
Tank inner diameter (m)	d_{in}	$[2.5-3.30]$
Hydrogen mass (kg)	m_{H_2}	$[300-1300]$
Cruise altitude (ft)	h_{cr}	$[25000-30000]$
Venting pressure (bar)	p_{vent}	$[2.00-6.00]$
Dormancy time (min)	t_{dorm}	$360\ (@ISA+15K)$

To assess the aircraft-level integration, a surrogate model was built using the aforementioned methodology, adopting four design variables, shown in Table 3 together with their variation ranges. The hydrogen tanks are housed just aft of the rear bulkhead as depicted in Figure 3, considering a non-integral configuration. A two-tank arrangement is adopted, where the secondary tank, placed in the fuselage tail cone, stores a constant hydrogen mass of 100 kg throughout the entire aircraft DOE analysis. Indeed, any hydrogen mass variation will be transferred to the primary section housed at the end of the fuselage constant-section region. Moreover, the tank diameter is maximised to ensure a contained aircraft centre of gravity excursion, while constrained by the fuselage diameter, which is fixed in the current study; the maximum tank diameter can be calculated as follows:

$$d_{\text{tank}} = d_{\text{fus}}(x_{\text{bkh}}) - 2t_{\text{wall}} \tag{4}$$

where $t_{\text{wall}} = 0.05$ m is the structural clearance from the fuselage wall.
For hydrogen-powered and hybrid-electric configurations, a dedicated geometry-convergence loop aims to match the total *hydrogen* fuel mass required by the mission with the fuselage length at each point of the DOE. The surrogate model is here employed to derive the overall tank geometry and mass by providing the total hydrogen mass stored in the primary tank and the remaining input

variables (provided in Table 3) of the current mission, while satisfying the tank diameter constraint. As a consequence, the fuselage length is updated to account for the primary tank length variation, only lengthening or shortening the fuselage cross-sectional region. The relative position of the horizontal and vertical tails respect to the fuselage length is kept the same for each fuselage update; therefore, to preserve the same volumetric coefficients, the tail plane surfaces are scaled accordingly by keeping a constant aspect ratio.

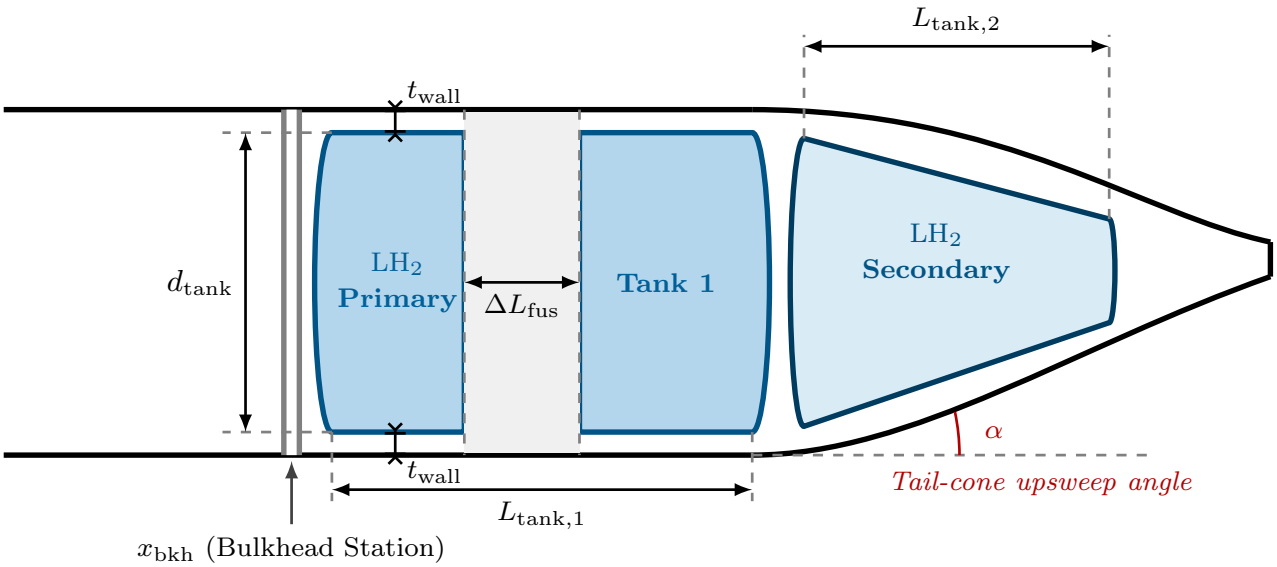


Figure 3 – Rear-fuselage hydrogen tank arrangement: fixed secondary conical-frustum tank and variable primary cylindrical tank. The fuselage length adapts at each outer geometry-loop iteration to accommodate the converged mission hydrogen requirement.

2.4 Constraint Evaluation and Performance Metrics

After convergence of each DOE point, the principal performance metrics are extracted and evaluated against the imposed TLARs. The enforced constraints are:

(i) maximum wing span: b [m]

(ii) maximum take-off field length: TOFL [m]

(iii) maximum landing field length: LFL [m]

(iv) maximum approach speed (CAS): V_{app} [kn]

(v) maximum MTOW: MTOW [kg]

(vi) maximum cruise Mach number: M_{cr} [–]

Design points violating any TLAR are classified as infeasible and excluded from optimum identification, but are retained in the response-surface database. Points yielding invalid values in key mass or performance metrics are additionally filtered out prior to response surface construction and counted separately as unconverged.

2.5 Response Surface Assembly and Constrained optimization

Following the completion of the DOE sweep, the evaluated outputs are assembled into a response-surface database providing a continuous map from any architecture-specific design vector ($\mathbf{x}_{\mathrm{K}} \in \mathscr{X}_{\mathrm{K}}$ for kerosene, $\mathbf{x}_{\mathrm{H}} \in \mathscr{X}_{\mathrm{H}}$ for hydrogen) to the corresponding aircraft performance characteristics — including block fuel mass — while simultaneously enabling feasibility assessment of each configuration against the prescribed TLARs.

The optimization utilizes a Sequential Quadratic Programming (SQP) algorithm. The objective function can be set to optimize the amount of energy carried on board, the total emissions during the design mission, or to find the best compromise solution that simultaneously minimizes both of the previous parameters. The objective function is evaluated through the interpolated response surface, whether all six TLAR constraints are enforced simultaneously as nonlinear inequality constraints. The optimization is initialized from the best feasible discrete DOE point and is bounded by the DOE grid extrema in each dimension. The solver settings are summarized in Table 4.

Table 4 – SQP solver configuration for the constrained optimization.

Parameter	**Value**
Algorithm	Sequential Quadratic Programming
Optimality tolerance	10^{-10}
Step tolerance	10^{-10}
Constraint tolerance	10^{-8}
Maximum function evaluations	5000
Maximum iterations	400

3. Aircraft Configurations and Top-Level Requirements

Six regional aircraft configurations are analyzed in this study, formed by the combination of two passenger capacities and three propulsion architectures:

- a 80-passenger and 100-passenger kerosene-powered aircraft with twin gas-turbine engines (configuration **K80** and **K100** respectively);
- a 80-passenger and 100-passenger hydrogen fuel-cell aircraft with four fuel-cell propulsion units and cryogenic rear-fuselage tanks (configuration **H80** and **H100** respectively);
- a 80-passenger and 100-passenger hybrid-electric aircraft combining kerosene gas-turbine and hydrogen fuel-cell propulsion, with cryogenic rear-fuselage hydrogen storage for a total of 2 propulsive units (configuration **KH80** and **KH100** respectively);

All configurations are reported in Figure 4, and all are designed for a 500 nm design mission range. The installation of fuel-cell systems, electric motors, and air-supply subsystems is modeled explicitly within the HEART framework.

3.1 DOE Parameter Ranges

The DOE parameter ranges for all six configurations are listed in Tables 5, 6, and 7. Wing planform area and aspect ratio are shared across all architectures; propulsion-power dimensions are activated or deactivated automatically according to the detected configuration, as described in Section 2.2.

Table 5 – DOE parameter ranges and number of levels — kerosene-powered configurations.

Design Variable	Symbol	Lower Bound	Upper Bound	Levels
Wing planform area	S	60 m^2	90 m^2	7
Wing aspect ratio	AR	11	14	4
Gas turbine engines power	P_{GT}	6 MW	8 MW	9

Table 6 – DOE parameter ranges and number of levels — hydrogen-powered configurations.

Design Variable	Symbol	Lower Bound	Upper Bound	Levels
Wing planform area	S	80 m^2	105 m^2	6
Wing aspect ratio	AR	11	14	4
Fuel-cell power (80 pax)	P_{FC}	6 MW	10 MW	5
Fuel-cell power (100 pax)	P_{FC}	8 MW	12 MW	5
Tank venting pressure	p_v	2 bar	6 bar	5

Table 7 – DOE parameter ranges and number of levels — hybrid-electric configurations.

Design Variable	Symbol	Lower Bound	Upper Bound	Levels
Wing planform area	S	85 m^2		1
Wing aspect ratio	AR	12		1
Gas-turbine engine power	P_{GT}	2 MW	5 MW	3
Fuel-cell system power		*Variable*		
Tank venting pressure	p_v	2 bar		1

3.2 Top-Level Aircraft Requirements

The TLARs enforced for the investigated configurations are summarized in Table 8. The maximum take-off weight (MTOW) limit differs between the kerosene- and hydrogen-powered variants to account for the greater structural and systems mass intrinsic to cryogenic propulsion architectures. Additionally, the cruise Mach number constraint allows for a reduced speed if the powertrain cannot provide sufficient power to reach Mach 0.50.

For the hybrid-electric configuration, the design space has been constrained. Specifically, the wing planform area and aspect ratio were fixed based on previous DOEs performed for both the kerosene and hydrogen configurations, balancing fuel savings with span limitations. Furthermore, the venting pressure is fixed at the minimum value specified in Table 3, as higher values negatively impacted the overall aircraft structural mass without yielding sufficient block fuel savings.

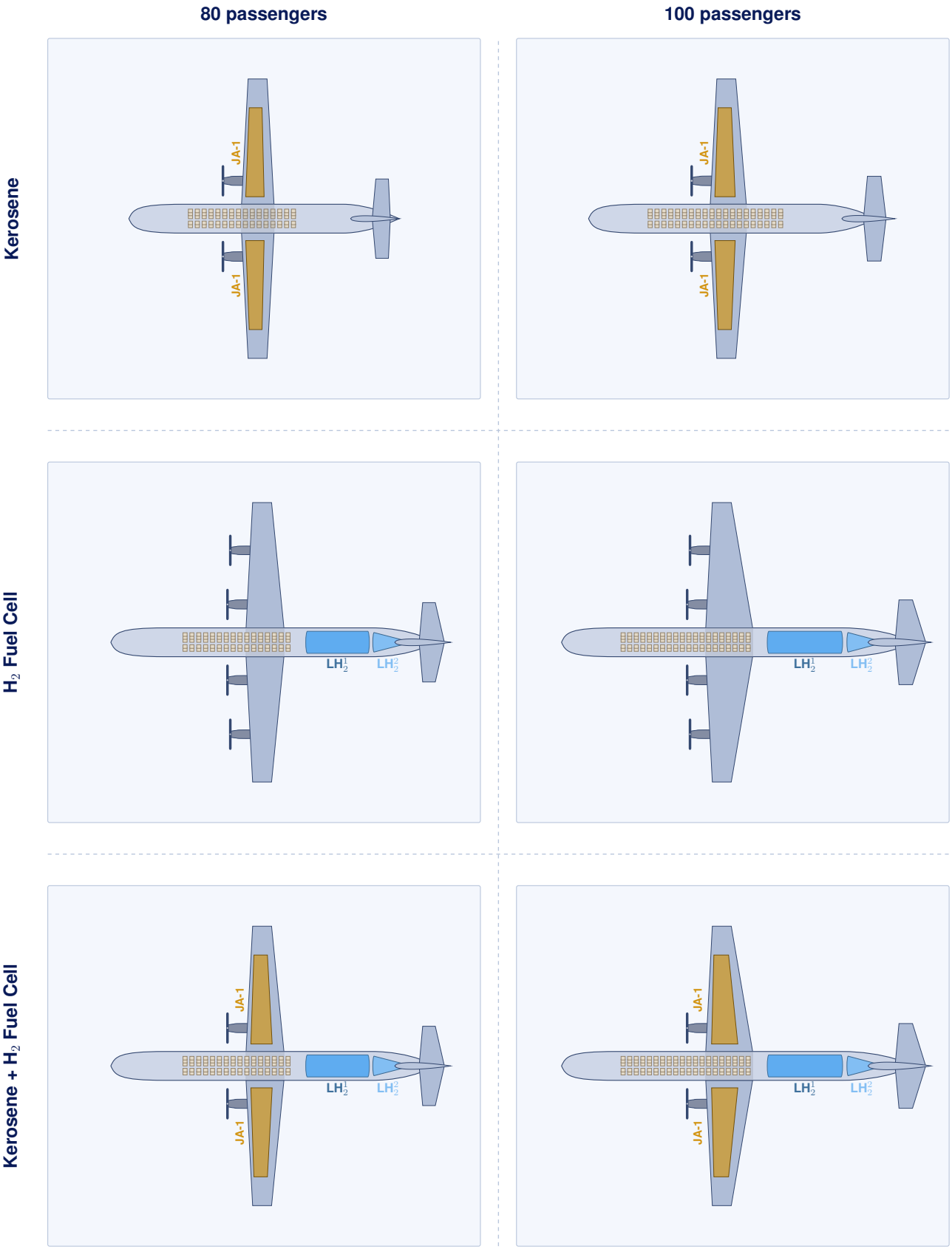


Figure 4 – A rough schematic comparison of the six aircraft configurations: kerosene (K80, K100), hydrogen fuel-cell (H80, H100), and hybrid-electric (KH80, KH100) variants. Fuselage elongation and additional nacelles on the hydrogen and hybrid configurations are shown indicatively.

Table 8 – Top-Level Aircraft Requirements for all aircraft configuration under investigation, reported in Figure 4

Constraint	Symbol	Bound	Limit		
			Kerosene	Hydrogen	Hybrid
Maximum wing span	b	$\leq$		36 m	
Max. take-off field length	TOFL	$\leq$		1350 m	
Max. landing field length	LFL	$\leq$		1350 m	
Max. approach speed (CAS)	V_{app}	$<$		120 kn	
Maximum cruise Mach number	M_{cr}	$\leq$		0.50	

4. Results and Discussion

This section presents the Design of Experiment (DOE) results, in terms of block fuel, obtained for each configuration shown in Figure 4. Additionally, using the method presented in Section 2.5, the optimal design parameters to minimise the block fuel are determined for all six configurations. This is followed by an evaluation of the actual energy stored on board, comparing kerosene-based, hydrogen-based, and hybrid-electric solutions, and identifying how the optimal energy required to complete the mission varies across architectures and payload classes.

4.1 DOE Results and Best-Aircraft Configurations

Using the design parameters defined in Table 5 - 7 several response surfaces, showing the block fuel behaviour, are presented in Figure 5 - 7. A preliminary screening was performed on the LH2 tank venting pressure (p_{vent}). The structural analysis demonstrated a monotonic trend: minimizing p_{vent} systematically reduces the tensile stresses on the cryogenic tank walls, thereby minimizing the shell thickness and the overall OEM. This negative aspect also outclass the favourable impact on the block fuel savings due to relaxed boil-off limitations, therefore, the venting pressure was locked at its minimum optimal value for the subsequent optimization phases, reducing the dimensionality of the search space.

The interaction between wing geometry and propulsive capabilities delineates a highly asymmetric design space. The transition from kerosene to LH2 profoundly alters aerodynamic feasibility, driving the configurations against different Top Level Aircraft Requirements (TLARs).

For the conventional kerosene configurations (K80 and K100), the boundaries of the feasible design space are primarily dictated by the trade-off between the cruise Mach number (M_{cruise}) requirement and the approach speed (V_{app}) limit. While smaller wing areas are beneficial for reducing cruise skin friction drag, they demand a higher maximum trimmed lift coefficient during landing, pushing V_{app} towards its upper allowable limit. Conversely, enlarging the wing area intrinsically increases the total wetted surface and aerodynamic drag. For a fixed installed propulsive power, this drag increment imposes a severe penalty on the maximum attainable flight speed. This phenomenon becomes particularly critical at the lower bounds of the investigated power envelope, where it acts as a primary sizing constraint.

Analyzing the block fuel contours, it is evident that oversizing the propulsion system leads to a significant increase in fuel consumption, with penalties reaching up to 15-20% due to lower throttle settings. Scaling the payload from 80 to 100 passengers negatively impacts the MTOW. For a given powertrain architecture and installed power, the increased mass extends the required ground roll distances; this magnifies the influence of the Take-Off Field Length (TOFL) constraint, which becomes a stringent limiting parameter for combinations of smaller wing areas and lower power, effectively eroding the bottom-left region of the design space. Finally, in both configurations, increasing the aspect ratio yields a positive impact on fuel savings due to reduced induced drag while enlarging the design space.

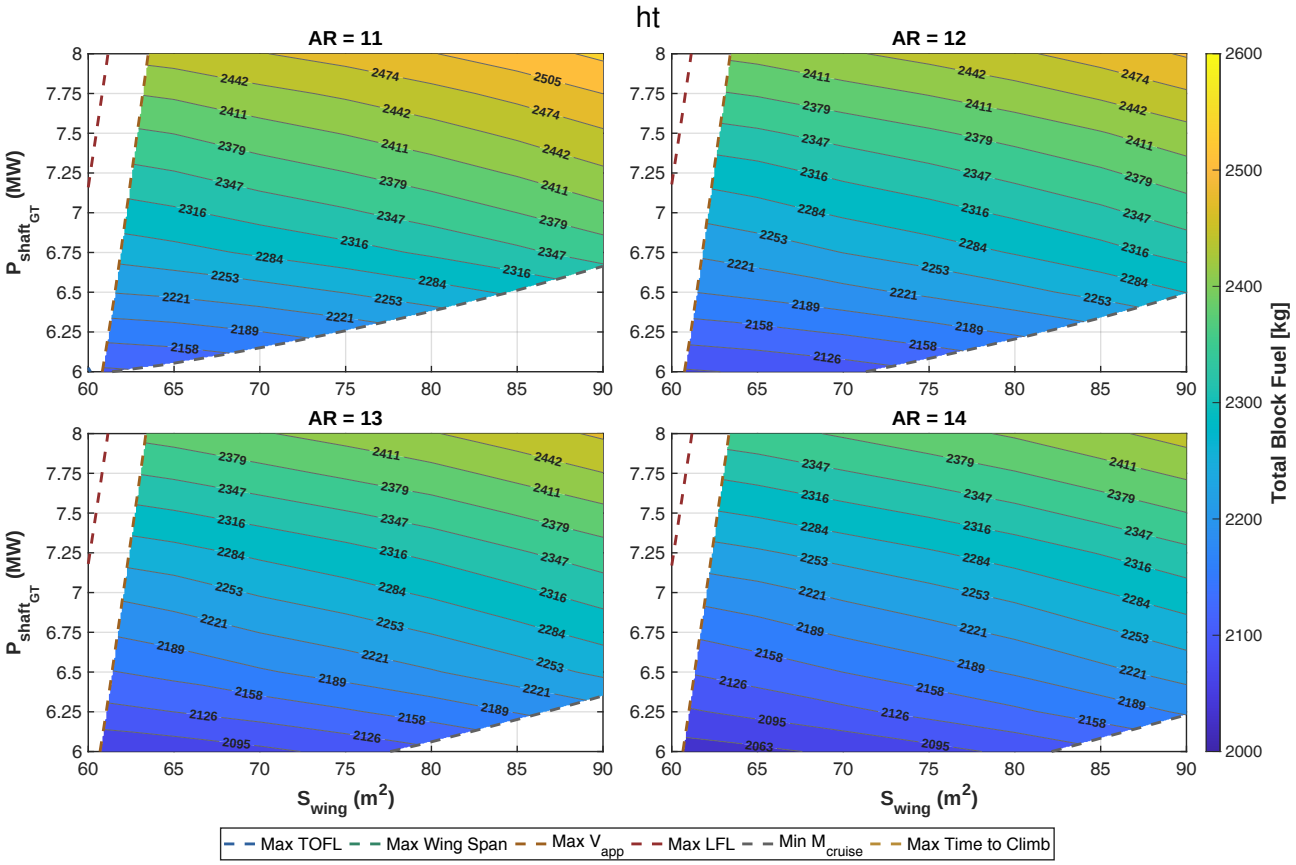


Figure 5 – Block fuel response surface of K80 aircraft configuration. The design variables are reported in Table 6. The dashed lines refer to the TLAR requirements, shaping the design space.

In liquid hydrogen (LH_2) architectures, the integration of unpressurized cryogenic tanks within the fuselage leads to a drastic increase in the total wetted area. The associated penalty in zero-lift drag ($C_{D,0}$) necessitates larger wing areas to sustain cruise conditions, fundamentally shifting the aircraft's sensitivity to field length Top-Level Aircraft Requirements (TLARs).
The most critical finding of the Design of Experiments (DoE) concerns the 100-passenger LH_2 configuration (H100). For this specific architecture, the feasible design space almost vanishes. This is attributed to a cascading weight penalty inherent to the low volumetric density of LH_2: accommodating 100 passengers requires a fuselage stretch that massively increases both structural mass and drag. Counteracting this requires larger wings and higher installed thrust, which iteratively inflates the MTOW, leading to the violation of Take-Off Field Length (TOFL) or approach speed (V_{app}) constraints. For these reasons, only the optimzed solution, reported in Table 9, has been reported, which highlights the higher wing surface and installer power required to satisfy the TLAR requirements.
From an energetic perspective, despite the higher aircraft masses in the hydrogen-powered configurations, the superior gravimetric specific energy of hydrogen compared to traditional kerosene results in a substantial reduction (almost 28 to 43% respectively, switching from 80 to 100 passenger aircraft configurations) in required block energy and a drastic decrease in block fuel mass. Finally, it is worth noting that the time-to-climb performance improves in the hydrogen configurations; these architectures benefit from the higher installed power levels required for takeoff and cruise, albeit at the cost of an increased MTOW.

4.2 Hybrid-Electric Architecture Sizing and Degree of Hybridization

To address the limitations of pure LH2 scaling, a hybrid-electric architecture, in particular a Turboelectric powertrain arrangement, was evaluated. To provide a consistent comparative baseline, this configuration was constrained to a fixed wing area and aspect ratio.

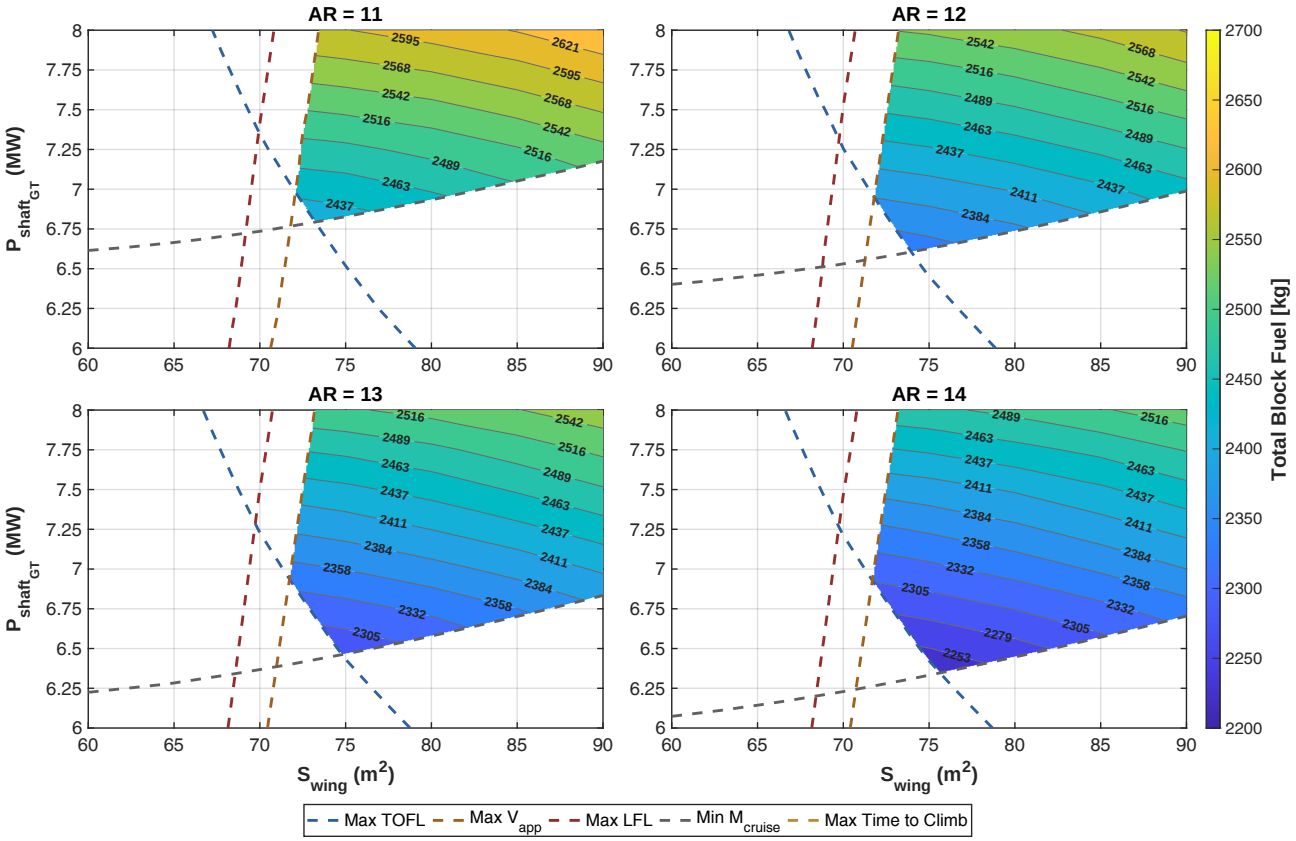


Figure 6 – Block fuel response surface of K100 aircraft configuration. The design variables are reported in Table 6. The dashed lines refer to the TLAR requirements, shaping the design space.

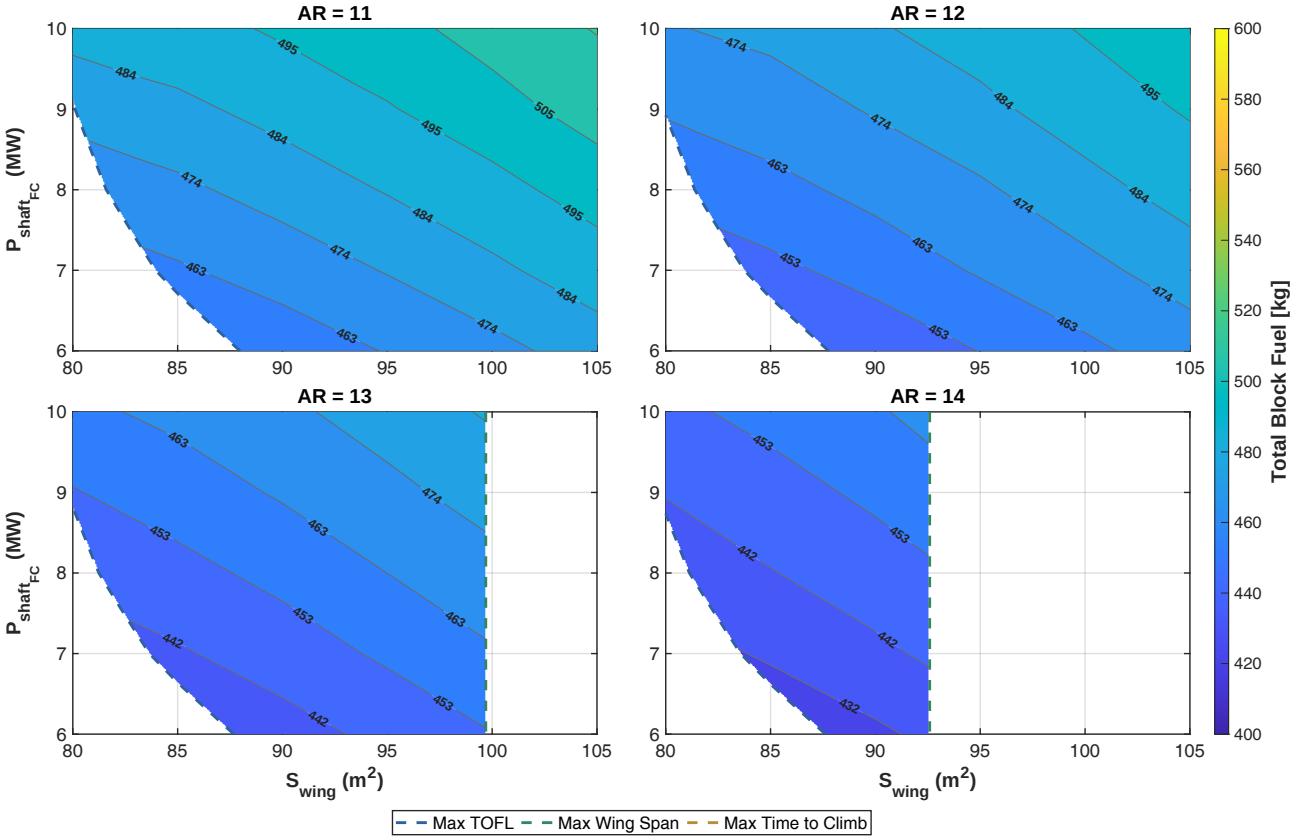


Figure 7 – Block fuel response surface of H80 aircraft configuration. The design variables are reported in Table 6. The dashed lines refer to the TLAR requirements, shaping the design space.

The selected wing area represents an optimal intermediate value derived from a trade-off between the highly loaded wings of the kerosene configurations and the larger surfaces required by the high-drag LH2 fuselage. Furthermore, the wing aspect ratio was deliberately constrained to $AR = 12$, despite aerodynamic models suggesting an optimum near 14. This multidisciplinary design choice was driven by two main factors: the first one is structural, which tries alleviate the overall structural penalties already generated by the gravimetric density of the additional electrical powertrain (Fuel Cells, motors, inverters). A higher aspect ratio would significantly increase the root bending moment, leading to structural weight penalties that would negate any aerodynamic drag reduction. Moreover, an AR of 12 ensures the aircraft comfortably clears wingspan limitation required by TLARs.

Following this assumptions, for both hybrid configurations, a DOE analysis was performed by imposing the gas turbine and fuel cell installed power as design variables. The suitable gas turbine values have been swept, and a series of hybridization levels ($\Phi = P_{FC}/(P_{FC} + P_{GT})$ have been evaluated as well. The optimized solutions are reported in Table 10. Switching from 80 to 100 passengers, the optimal hybridization level drop of almost 9%, in order to cope with the increased fuselage length and overall MTOW increment; indeed, the specific power of gas turbine considered is almost 5 times higher than the fuel cell counterpart, meaning a lower weight penalty in increasing the gas turbine installed power instead of the fuel cell one. On the other hand, the energy contents slightly differs, but since the gas turbine contribution gains more importance, the emissions, measured in $CO_{2_{eq}}$ rise of almost 17%. At last, it is worth noting that the 80 pax hybrid configuration (KH80) is able to satisfy all TLAR requirements, whereas the 100 passenger configuration is not able to satisfy the TOFL requirements due to a lower total power installed and increased MTOW, These consideration suggests that a higher wing area should have been consider, in order to reduce the wing loading and, consequently, the overall TOFL, but providing additional drag and block fuel.

Table 9 – Comparison of optimized aircraft design variables and aircraft performance for the kerosene-powered (K80 and K100) and hydrogen-powered (H80 and H100) configurations, reported in Figure 4. The objective function is the block fuel, with non linear constraints set by the TLAR requirements reported in Table 8.

	K80	**K100**	**H80**	**H100**
Wing surface S (m^2)	62.0	71.8	81.1	110.4
Aspect ratio AR	14.0	14.0	14.0	11.7
Installed power (P_{shaft}) (MW)	7.00	7.0	8.0	11.0
TOFL (m)	1221	1342	1350	1350
LFL (m)	1328	1329	1245	1246
MTOW (kg)	28674	33222	33776	46161
Time to Climb (min)	17.2	14.6	12.8	12.6
Block fuel (kg)	2873	3001	584	773
Block Energy (MJ)	1.23e5	1.29e5	7.0e4	9.27e4

5. Conclusions

This study conducted a comparative and multidisciplinary design optimization analysis for regional aircraft, evaluating the impact of different propulsive architectures and payload capacities. Six distinct configurations were analyzed, comparing conventional kerosene propulsion (K80, K100), liquid hydrogen propulsion (H80, H100), and hybrid fuel cell-gas turbine architectures for the 80- and 100-passenger classes.

The most prominent finding of the research is that the impact of increasing the number of passengers is non-linear and varies drastically depending on the chosen propulsive technology. While for conventional configurations the transition from 80 to 100 seats implies a predictable and proportional scaling, for alternative propulsion architectures the payload increment acts as a catalyst for critical issues, pushing current technologies to the boundaries of design feasibility.

Table 10 – Comparison of optimized variables for Kerosene and Hydrogen (Fuel Cell) aircraft configurations.

Kerosene Configurations	**KH80**			**KH100**		
	Energy (MJ)	Emissions ($CO2_{eq}$)	Pareto	Energy (MJ)	Emissions ($CO2_{eq}$)	Pareto
Wing surface S (m^2)		85			85	
Aspect ratio AR		12			12	
Installed GT power (P_{GT}) (MW)		3.67			4.00	
Installed FC power (P_{FC}) (MW)		7.28			5.74	
Hybridization factor ($\%$)		66.5			58.9	
TOFL (m)		1350			1498	
LFL (m)		1315			1325	
MTOW (kg)		38895			39322	
Time to Climb (min)		13.0			18.3	
	9.44e4	3412		1.00e5	4019	

The key findings emerging from the comparison of the six configurations can be summarized as follows:

- **Conventional Kerosene Configurations** As expected, the capacity increase results in a moderate rise in Maximum Take-Off Weight and Block Energy. These configurations easily close the design space, fulfilling the Top-Level Aircraft Requirements (TLARs) related to field performance (Take-Off Field Length, TOFL) and approach speed (V_{app}) without requiring excessive wing or propulsive oversizing.
- **Liquid Hydrogen Configurations** The integration of unpressurized cryogenic tanks within the fuselage generates a severe volumetric penalty. The increase in wetted area and the consequent parasite drag ($C_{D,0}$) necessitate significantly larger wings. The main key finding presents the H80 configuration as a suitable alternative to kerosene-powered aircraft with the same number of passengers, although the overall design space collapse for the H100 configuration. The fuselage stretch required to accommodate the 20 extra passengers triggers a cascading weight penalty: the heavier structure demands more thrust and a larger wing area to meet TOFL and V_{app} constraints, causing the MTOW to spike disproportionately compared to the H80 variant. However, from an energetic standpoint, the high gravimetric specific energy of LH_2 guarantees a drastic reduction in Block Energy for both configurations compared to conventional aircraft.
- **Hybrid Configurations** The analysis highlighted how the coupling between gas turbines and fuel cells is strongly constrained by the low specific power of the fuel cells and severe thermal management requirements. The crucial key finding in this domain is the necessary reduction of the hybridization level (Φ) as aircraft size increases. In the transition from 80 to 100 passengers, the optimizer is forced to lower the percentage of power delivered by the fuel cells. Maintaining a high level of hybridization for 100 passengers would entail unacceptable propulsive system mass, whose additional drag would irretrievably violate takeoff and climb TLARs. To successfully close the Hybrid 100 design, the system must rely more heavily on the power-dense gas turbines, or higher wing surfaces with the risk to break the wing span limitation.

In summary, while the 80-passenger class offers a flexible design space that allows for the successful exploration of both LH_2 and highly electrified hybrid solutions, the 100-passenger threshold exposes the current physical limits of these technologies. To make zero- or low-emission 100-seat configurations competitive, future research must focus on technologies capable of drastically increasing the

power density of onboard systems (both fuel cells and cooling systems) and on highly integrated aerodynamic solutions to mitigate the volumetric penalties of hydrogen.

6. Contact Author Email Address

The contact author for this paper is Salvatore Trepiccione: salvatore.trepiccione@unina.it.
Additional authors may be reached at: giuseppe.melone@unina.it, mario.distasio@unina.it, fabrizio.nicolosi@unina.it.

7. Copyright Statement

The authors confirm that they, and/or their company or organization, hold copyright on all of the original material included in this paper. The authors also confirm that they have obtained permission, from the copyright holder of any third party material included in this paper, to publish it as part of their paper. The authors confirm that they give permission, or have obtained permission from the copyright holder of this paper, for the publication and distribution of this paper as part of the ICAS proceedings or as individual off-prints from the proceedings.

8. Acknowledgments

The research presented in this paper has been performed in the framework of the HERA project (Hybrid Electric Regional Aircraft) and has received funding from the European Union Clean Aviation Program under grant agreement n° 101102007.





Co-funded by
the European Union



References

[1] D.S. Lee, D.W. Fahey, A. Skowron, M.R. Allen, U. Burkhardt, Q. Chen, S.J. Doherty, S. Freeman, P.M. Forster, J. Fuglestvedt, A. Gettelman, R.R. De León, L.L. Lim, M.T. Lund, R.J. Millar, B. Owen, J.E. Penner, G. Pitari, M.J. Prather, R. Sausen, and L.J. Wilcox. The contribution of global aviation to anthropogenic climate forcing for 2000 to 2018. *Atmospheric Environment*, 244:117834, 2021.

[2] V. Marciello, M. Ruocco, F. Nicolosi, and M. Di Stasio. Market analysis, TLARs selection and preliminary design investigations for a regional hybrid-electric aircraft. In *Proc. 33rd Congress of the International Council of the Aeronautical Sciences (ICAS)*, Stockholm, Sweden, September 2022.

[3] Airbus. ZEROe: our hydrogen-powered aircraft. Airbus online, `https://www.airbus.com/en/innovation/energy-transition/hydrogen/zeroe-our-hydrogen-powered-aircraft`, 2026. Accessed 05 January 2026.

[4] Aerospace Technology Institute (ATI). FlyZero: Zero-carbon emission aircraft concepts. Technical Report FZO-AIN-REP-0007, Aerospace Technology Institute, 2022. Accessed 05 January 2026.

[5] A. De Marco, M. Di Stasio, P. Della Vecchia, V. Trifari, and F. Nicolosi. Automatic modeling of aircraft external geometries for preliminary design workflows. *Aerospace Science and Technology*, 8, 2020.

[6] A. De Marco, V. Trifari, F. Nicolosi, and M. Ruocco. A simulation-based performance analysis tool for aircraft design workflows. *Aerospace*, 7(11), 2020.

[7] M. Di Stasio, F. Nicolosi, G. Melone, and V. Cusati. Conceptual design and technology sensitivity analysis of a fuel cell short-range aircraft. In *Proc. 2025 AIAA AVIATION Forum*, Las Vegas, Nevada, July 2025.

[8] P. Prajwal, P.D. Ciampa, P. Della Vecchia, D. Ciliberti, M. Voskuij, D. Charbonnier, A. Jungo, M. Zhang, M. Fioriti, K. Anisimov, and A. Mirzoyan. Model based collaborative design & optimization of blended wing body aircraft configuration: AGILE EU project. In *Proc. 2018 Aviation Technology, Integration, and Operations Conference*, Atlanta, Georgia, June 2018.

[9] J.H. Bussemaker, P.D. Ciampa, J. Singh, M. Fioriti, C. Cabaleiro, Z. Wang, D.M.J. Peeters, P. Hansmann, P. Della Vecchia, and M. Mandorino. Collaborative design of a business jet family using the AGILE 4.0 MBSE environment. In *Proc. 2022 AIAA AVIATION Forum*, Chicago, Illinois, June 2022.

[10] U. Rischmüller, A. Lessis, P. Egerer, and M. Hornung. Conceptual design of a hydrogen-hybrid dual-fuel regional aircraft retrofit. *Aerospace*, 11(2), 2024.

[11] V. Palladino, N. Bartoli, V. Pommier-Budinger, E. Benard, P. Schmollgruber, and A. Jordan. Optimization of a hydrogen-based hybrid propulsion system under aircraft performance constraints. *Chinese Journal of Aeronautics*, 36(5):41–56, 2023.

[12] M. Fioriti, C. Cabaleiro, T. Lefebvre, P. Della Vecchia, M. Mandorino, S. Liscouet-Hanke, A. Jeyaraj, G. Donelli, and A. Jungo. Multidisciplinary design of a more electric regional aircraft including certification constraints. In *Proc. 2022 AIAA AVIATION Forum*, Chicago, Illinois, June 2022.

[13] P. Aliberti, C. Simone, P. Addesso, G. De Piano, F. Donsi, A. Galdi, L. Maritato, R. Pantani, C. Pianese, P. Polverino, F. Postiglione, and M. Sorrentino. Fuel cells in aviation: challenges to power the future of flight. *Energy Conversion and Management: X*, 2025.

[14] C. Winnefeld, T. Kadyk, B. Bensmann, U. Krewer, and R. Hanke-Rauschenbach. Modelling and designing cryogenic hydrogen tanks for future aircraft applications. *Energies*, 11(1):105, 2018.

[15] Deutsches Institut für Normung (DIN). AD 2000-Merkblatt B 6: Cylindrical shells subjected to external overpressure. Technical report, DIN, Berlin, Germany, 2020.

[16] R. C. Parello, E. Benard, Y. Gourinat, and S. Defoort. Design and integration of a liquid hydrogen tank on an aircraft. In *Proceedings of the AIAA SciTech Forum*, Orlando, FL, USA, 2024. AIAA Paper 2024-2638.

[17] D. Verstraete. The potential of liquid hydrogen for long range aircraft propulsion. In *Proceedings of the 14th AIAA Aviation Technology, Integration, and Operations Conference*, 2009.